Extended Abstracts of the 2008 International Conference on Solid State Devices and Materials, Tsukuba, 2008, pp. 230-231

J-1-5

Electrical Characteristics of $TiO_2/Al_2O_3/TiO_2$ Stacked Films

Hikaru Hara[1], Masami Tanioku[2], Masaki Yamato[1] and Takamaro Kikkawa[1]

[1]Research Institute for Nanodevice and Bio Systems, Hiroshima University,
1-4-2 Kagamiyama, Higashi-Hiroshima, Hiroshima 739-8527, Japan
Phone: +81-82-424-6265 E-mail: hikaru-hara@hiroshima-u.ac.jp, kikkawat@hiroshima-u.ac.jp
[2]Elpida Memory, Inc.,
7-10 Yoshikawakogyodanchi, Higashi-Hiroshima, Hiroshima 739-0198, Japan

1. Introduction

It becomes very difficult for gigabit dynamic random access memories (DRAM's) to keep sufficient capacitance per unit cell. Therefore, it is needed for 40 nm technology to satisfy small equivalent oxide thickness (EOT) less than 0.5 nm and low leakage current less than 10^{-8} A/cm^2. To satisfy these requirements, we focus on two dielectric materials such as TiO_2 having larger dielectric constant but smaller band-gap and Al_2O_3 having larger band-gap but lower dielectric constant [1]. In this study, we investigated the leakage current characteristics of TiO_2 and Al_2O_3, and the electrical characteristics of Al_2O_3-TiO_2 mixed and stacked structures.

2. Experiment

Metal-Insulator-Metal (MIM) capacitor was formed on SiO_2/Si substrates. Platinum (Pt) was deposited as both top (ϕ=1.6 mm) and bottom electrodes. TiO_2 and Al_2O_3 films were deposited by RF magnetron sputtering by use of Al_2O_3 and TiO_2 targets, respectively. The gas mixture ratio of Ar and O_2 was Ar:O_2=1:1. The substrate temperature was 300°C. RF powers of sputtering for Al_2O_3 and TiO_2 were 70 W and 150 W, respectively. The post-deposition annealing in O_2 ambient was performed at the temperature of 600°C.

3. Results and discussion

Figure 1 shows equivalent oxide thickness (EOT) versus physical thickness for TiO_2 film. From this slope, relative dielectric constant of TiO_2 was calculated to be approximately 88.4. The dielectric constant of TiO_2 decreased with decreasing the physical thickness (Fig. 2). Figure 3 shows physical thickness dependence of leakage current density versus electric field. Leakage current modes were distributed by the physical thickness such as thick film (more than 40 nm), thin film (6.7-17.7 nm) and very thin film (less than 5.4 nm). A crystalline peak due to rutile phase of TiO_2 was observed in the films whose thicknesses were greater than 37.4 nm (Fig. 4). On the other hand, the films which were less than 18.2 nm had no peak due to TiO_2. Therefore, because of crystallization, 40 nm-thick TiO_2 had large leakage current. Figures 5 and 6 show temperature dependences of leakage current for 17.7 and 5.4-nm thick TiO_2 films, respectively. For each thickness of the TiO_2 film, the leakage current depends on the temperature at high electric field, significantly. The leakage current of Frenkel-Poole (FP) emission (J_{FP}) is expressed as

$$J_{FP} \sim E \exp\left[\frac{-q(\Phi_B - \sqrt{qE/\pi\varepsilon_i}}{kT}\right], \qquad (1)$$

where E is the electric field, q is the unit electric charge, Φ_B is the barrier height, ε_i is the insulator permittivity and k is the Boltzmann constant. The Frenkel-Poole plot yields a straight line at high electric field and can derive a more favorable ε_i (around $1.4\varepsilon_0$) than that of Schottky plot as shown in Fig. 7 [2]. Therefore, the conduction mechanism of 17.7-nm thick TiO_2 film is FP emission at high electric field. Figure 8 shows Arrhenius plot of FP emission for 17.7-nm thick TiO_2 film. From these slopes, the Φ_B of FP emission for 17.7-nm thick TiO_2 was estimated to be 1.38 eV (Fig. 9). The Φ_B of FP emission for 40 and 4.5 nm-thick TiO_2 were also estimated to be 1.13 and 1.30 eV, respectively. Though the Φ_B of 5.4 nm-thick TiO_2 was high, leakage current was large at low electric field due to direct tunneling current. Temperature dependence of leakage current for Al_2O_3 film is shown in Fig. 10. The leakage current of Al_2O_3 film had little dependence on the temperature at high electric field. The plot of ln(J/E^2) versus $1/E$ became a straight line as shown in Fig.11. Therefore, the conduction mechanism at high electric field is Fowler-Nordheim (F-N) tunneling [1]. The electrical characteristics of $TiO_2/Al_2O_3/TiO_2$ stacked films were investigated. Figure 12 shows Al content dependence of leakage current density versus electric field. The leakage current of the $TiO_2/Al_2O_3/TiO_2$ stacked film decreased with increasing the Al content. Electric field (@ J=10^{-8} A/cm^2) versus dielectric constant for $TiO_2/Al_2O_3/TiO_2$ stacked film is shown in Fig. 13. The electric field (@ J=10^{-8} A/cm^2) decreased with increasing the dielectric constant. The maximum effective dielectric constant was 51. Figure 14 shows voltage (@ J=10^{-8} A/cm^2) versus EOT for several film structures. The $TiO_2/Al_2O_3/TiO_2$ stacked film had high electric field (@ J=10^{-8} A/cm^2) in comparison with the other structures having the same EOT. Consequently, the EOT of 0.58 nm with leakage current of 10^{-8} A/cm^2 at 0.93 V was obtained by use of $TiO_2/Al_2O_3/TiO_2$ structure with thickness of 3.5/0.6/3.5 nm.

4. Conclusion

The leakage current mechanisms of TiO_2 and Al_2O_3 were Frenkel-Poole emission and F-N tunneling, respectively. Since direct tunneling was dominant for TiO_2 film with the thickness less than 5.4 nm, the minimum EOT of 0.58 nm was obtained by use of $TiO_2/Al_2O_3/TiO_2$ structure.

References

[1] Lu *et al.*, Appl. Phys. Lett. 90,082911 (2007)

[2] M. Yamato *et al.*, Jpn. J. Phys., Vol. 43, No. 8A (2004)

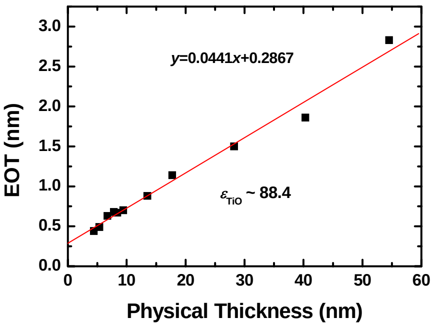

Fig. 1. EOT versus physical thickness for TiO_2 film.

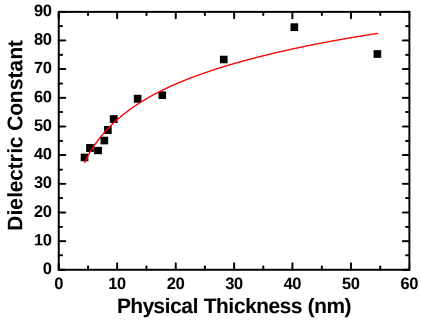

Fig. 2. Dielectric constant versus physical thickness for TiO_2 film.

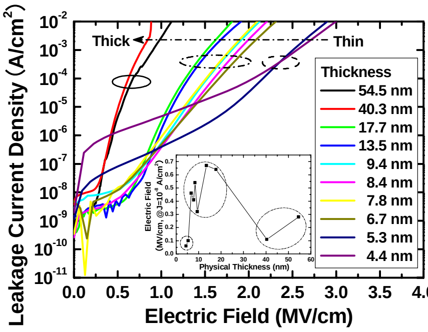

Fig. 3. Physical thickness dependence of leakage current density versus electric field.

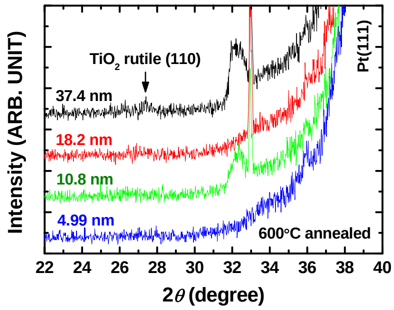

Fig. 4. Physical thickness dependence of X-ray diffraction spectra for TiO_2 film.

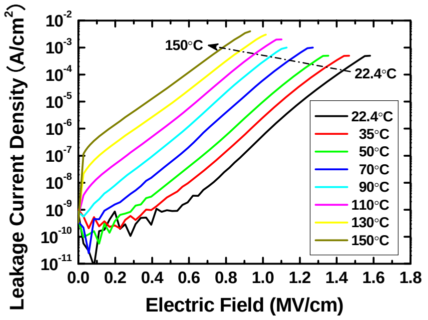

Fig. 5. Temperature dependence of leakage current for 17.7-nm thick TiO_2 film.

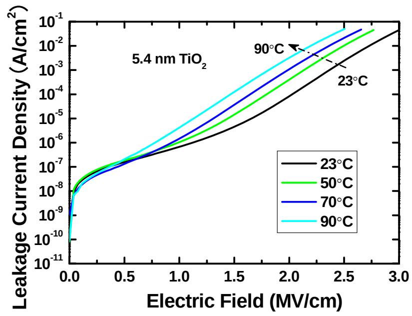

Fig. 6. Temperature dependence of leakage current for 5.4-nm thick TiO_2 film.

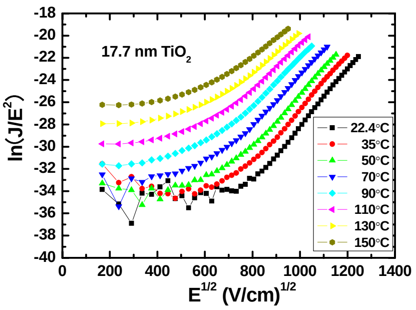

Fig. 7. Frenkel-Poole plot for 17.7-nm thick TiO_2 film.

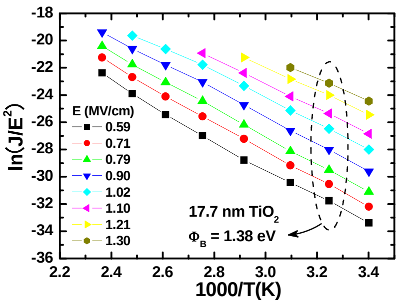

Fig. 8. Arrhenius plot of Frenkel-Poole emission for 17.7-nm thick TiO_2 film.

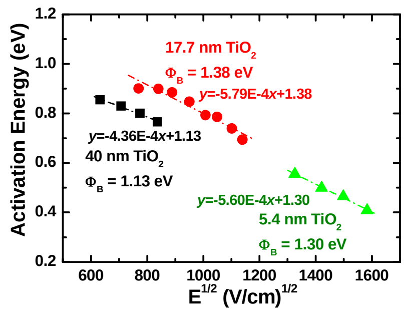

Fig. 9. Activation energy versus $E^{1/2}$ for each thickness of TiO_2 film.

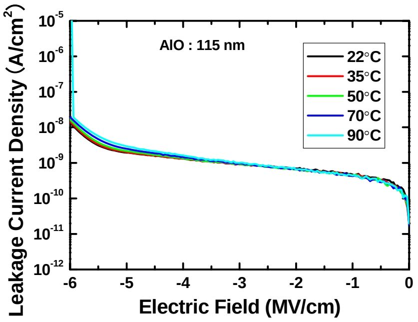

Fig. 10. Temperature dependence of leakage current for Al_2O_3 film.

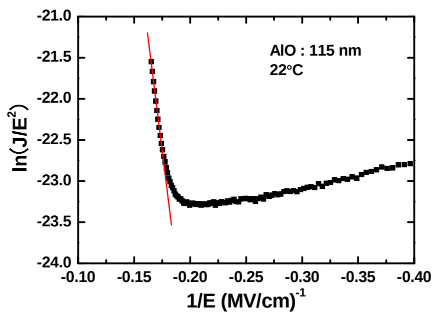

Fig. 11. Fowler-Nordheim (F-N) plot for Al_2O_3 film.

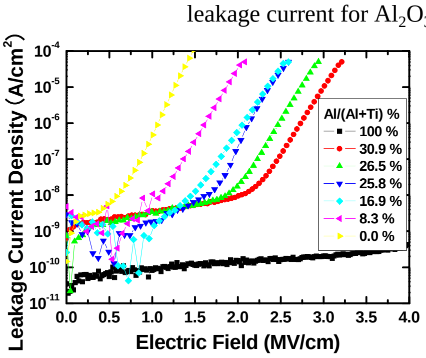

Fig. 12. Al content dependence of leakage current density versus electric field.

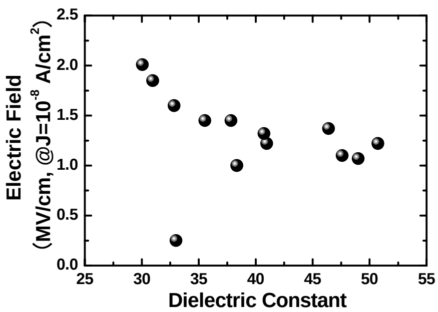

Fig. 13. Electric field (@ J=10^{-8} A/cm^2) versus dielectric constant for $TiO_2/Al_2O_3/TiO_2$ film.

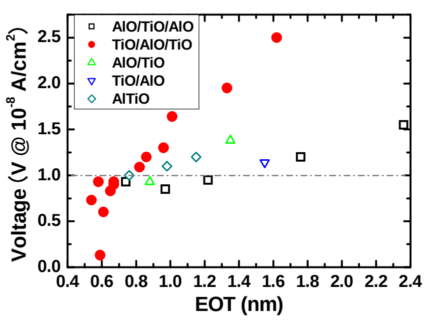

Fig. 14. Voltage (@ J=10^{-8} A/cm^2) versus EOT for several film structures.